Article

Not peer-reviewed version

Multivariate Calibration for Selective Analysis of Hydrogen Sulfide and Carbon Monoxide with Thermal Modulation of the SnO_2–PdO Sensor

Alexey Shaposhnik *, Pavel Moskalev, Alexey Vasiliev, Kirill Oreshkin, Alexey Zviagin, Elena Vysotskaya, Sergey Yu. Turishchev, Iuliia Kakuliia

Posted Date: 28 July 2025

doi: 10.20944/preprints202507.2112.v1

Keywords: metal oxide sensor; multivariate calibration; selective analysis; temperature modulation; hydrogen sulfide; carbon monoxide

 doi:10.20944/preprints202507.2112.v1

Article

Multivariate Calibration for Selective Analysis of Hydrogen Sulfide and Carbon Monoxide with Thermal Modulation of the SnO_2–PdO Sensor

Alexey Shaposhnik [1,*], Pavel Moskalev [2], Alexey Vasiliev [3], Kirill Oreshkin [1], Alexey Zviagin [1], Elena Vysotskaya [1], Sergey Turishchev [4] and Iuliia Kakuliia [4]

[1] Voronezh State Agrarian University, Voronezh, Russia
[2] Moscow State University of Technology "STANKIN", Moscow, Russia
[3] Dubna State University, Dubna, Russia
[4] Voronezh State University, Voronezh, Russia
* Correspondence: a.v.shaposhnik@gmail.com

Abstract

Multivariate data processing during thermal modulation of the SnO_2–PdO gas sensor was performed using the multivariate calibration (MC) method. We propose to supplement this method with a procedure that allows solving problems of both quantitative and qualitative analysis. The advantage of the extended method (Multivariate Calibration for Selective Analysis, MCSA) compared to other methods is its modest requirements for computing resources, which allows it to be easily implemented on standard microcontrollers. The MCSA method opens up the prospect of creating compact gas analyzers of a new generation capable of selective gas analysis in hard-to-reach places in an autonomous mode. The implementation of the MCSA method was demonstrated using the example of selective determination of hydrogen sulfide and carbon monoxide by a sensor whose temperature periodically changed from 100 to 450 °C. The training sample data were transformed by the MCSA method, which allowed for successful qualitative and quantitative analysis of the test sample data.

Keywords: metal oxide sensor; multivariate calibration; selective analysis; temperature modulation; hydrogen sulfide; carbon monoxide

1. Introduction

The two main tasks of gas sensor analysis are to increase their sensitivity and selectivity. One of the most effective ways to solve these problems is to switch from steady-state operation modes of a metal oxide sensor to modulating its temperature. As we have shown earlier, a sharp change in temperature can lead to an increase in sensor sensitivity by two to three orders of magnitude [1]. In addition, temperature modulation can also increase the selectivity of the analysis performed by the sensor [2–5].

There are two fundamentally different approaches to increasing the selectivity of the analysis. One of them is to create highly selective sensors that have a significant sensitivity ratio between the target gas and the components of the system interfering with the determination. For example, when determining hydrogen sulfide, the cross-sensitivity was 5–6 orders of magnitude with respect to hydrogen, carbon monoxide and ammonia [6]. In this case, the term "highly selective sensor" can be used. The second way to increase selectivity is to use several sensors combined into an "electronic nose" system [7–11]. The third way is temperature modulation of a low-selectivity sensor [12–20]. The first way is preferable because the use of highly selective sensors allows one to avoid the influence of any interfering components. At the same time, temperature modulation also has its

 doi:10.20944/preprints202507.2112.v1

advantages, including, for example, the possibility of selectively determining different gases and even gas mixtures [1,5] by a single low-selectivity sensor.

Most of these studies used a sinusoidal change in the sensor temperature [3,21–23] or a sawtooth change in its temperature [18]. The pulse mode with a sharp heating of the sensor also has its advantages. The first advantage is lower energy consumption by the sensor in the measurement cycle. The second advantage is the ability to sharply activate the catalyst at a time when the gas has not yet had time to desorb from the surface, which helps to increase the sensitivity of the sensor. In some studies, a feedback mechanism was used to increase sensitivity – the sensor temperature changed during the experiment depending on its resistance [19,24]. To increase sensitivity, temperature modulation of the sensor can also be combined with its light modulation due to UV radiation [25].

Each measurement cycle in the temperature modulation mode forms a vector data array, which can be similar to the vector data array of a multisensor system – an "electronic nose". Measurements obtained by one sensor at different points in time of the measurement cycle are similar to measurements obtained by different sensors at the same point in time, so they can be processed by the same methods that are used for the "electronic nose"– the principal component method, artificial neural networks, etc. At the same time, there are fundamental differences between the multidimensional data obtained by one sensor in temperature modulation and the multidimensional data of the sensor array of the "electronic nose". A single sensor does not form an independent set of components, but a correlated time series, allowing us to trace the functional relationship between the electrical resistance and the temperature of the sensor (in time from the beginning of the cycle). This opens up the possibility of using chemometric methods different from those used in "electronic nose" type systems [5].

In many previously published works, the authors used the Fourier transform [2,26–28] and the wavelet transform [23,26,29]. However, the study of these approaches did not lead to the creation of selective gas analyzers. Firstly, it was not possible to develop clear algorithms for selective analysis that could be implemented in devices. Secondly, these transformations, which are easily implemented by computer processors or specialized microchips, are not suitable for creating compact gas analyzers based on the use of simple mass-produced microcontrollers. In this work, a new method for processing multidimensional data developed by us was used to process multidimensional data, which combines high efficiency with simplicity of software implementation.

Improving the accuracy of analysis when using multivariate data can be achieved by using multivariate calibration algorithms [30–32]. Typically, this method of processing vector data is used only for quantitative analysis [33–35]. Currently, new methods for synthesizing metal oxide materials with increased chemisorption activity are being developed to create next-generation semiconductor sensors [36–39]. Sol-gel synthesis is most often used to solve practical problems, and SnO_2 continues to be the most common sensor material. Sensors based on it with palladium additives are widely used for commercial purposes and are the objects of further scientific research [40–44].

2. Materials and Methods

2.1. Synthesis and Characterization of Tin Dioxide Nanopowder

Sol-gel synthesis was used to create the gas-sensitive layer of the sensor. The first stage consisted of obtaining a highly dispersed sol of tin acid H_2SnO_3 by reacting tin (IV) acetate $Sn(CH_3COO)_4$ with a concentrated solution of ammonia NH_3. In the second stage, tin acid H_2SnO_3 was isolated by centrifugation and dried at a temperature of 120 °C. In the third stage, the obtained tin acid powder was calcined at a temperature of 500 °C, as a result of which tin acid H_2SnO_3 decomposed to tin dioxide nanopowder SnO_2 [5].

Transmission electron microscopy was used to evaluate the geometric dimensions of the nanoparticles of the tin dioxide SnO_2 used. The Carl Zeiss Libra 120 microscope was used. Characterization of SnO_2 tin dioxide nanopowder was performed by X-ray Diffraction (XRD) using an ARL X`TRA device operating in Bragg-Brentano geometry. The XRD patterns registration was

 doi:10.20944/preprints202507.2112.v1

performed in the θ-θ mode, the samples were placed on silicon substrates with a "zero background". An X-ray tube with a copper anode (CuKα) was used as a source, discrimination of inelastically scattered radiation was performed by a semiconductor energy-dispersive detector with a resolution of 250 eV with a cooler on Peltier elements. To eliminate reflections from the substrate, the samples were tilted relative to the primary beam by 5°. The LaB_6 sample was used as an instrumental standard. The obtained diffraction patterns were decoded using the Powder Diffraction File (PDF-2) database.

2.2. Production of Gas-Sensitive Material SnO_2–PdO

At the first stage, tetraamminepalladium (II) nitrate $[Pd(NH_3)_4](NO_3)_2$ was added to nanodispersed tin dioxide SnO_2. At the second stage, the resulting nanopowder was mixed with a solution of ethylcellulose in terpineol to obtain a paste, which was applied to a special dielectric substrate containing platinum electrodes and a platinum heater. At the third stage, the substrate with a thin layer of paste applied to it was calcined at a temperature of 750 °C, as a result of which a gas-sensitive layer SnO_2–PdO was formed from the paste, which included 97% SnO_2 and 3% PdO (by weight) [5]. At the fourth stage, after the formation of the gas-sensitive layer, the sensor was soldered to the TO-8 housing (see Figure 1).

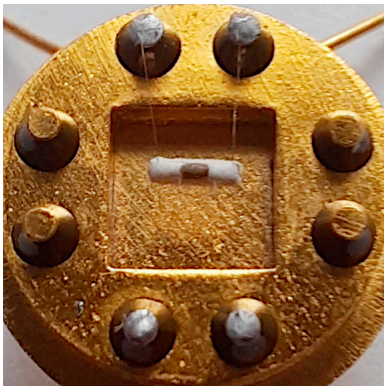

Figure 1. General view of the sensor soldered in the TO-8 housing.

2.3. Experimental Methodology with the Manufactured Gas Sensor

In this work, we used calibration gas mixtures of hydrogen sulfide H_2S with synthetic air, carbon monoxide CO with synthetic air, and hydrogen H_2 with synthetic air with concentrations of 10 and 200 ppm. The required concentrations were created by mixing the flows of the calibration gas mixture and synthetic air using a set of gas pressure regulators and mass flow controllers Bronkhorst and Eltochpribor.

To create a mixture of ethanol C_2H_5OH vapors with synthetic air, a special setup was used, which contained a 150 ml macro syringe, the piston of which moved automatically at a controlled speed. The required number of drops of ethanol solution in water were added to the macro syringe using a chromatographic syringe (1 μl). After equilibrium was established in the macro syringe chamber, the piston slowly pushed the gas mixture into the tee, where it was further diluted with synthetic air.

At the beginning of each measurement cycle, the manufactured sensor was heated from 100 °C to 450 °C over a period of 2 seconds, and then cooled from 450 °C to 100 °C over a period of 13 seconds. The measurement cycles lasting 15 seconds were continuously repeated. Figure 2 shows the change in sensor temperature over two measurement cycles (curve 1).

 doi:10.20944/preprints202507.2112.v1

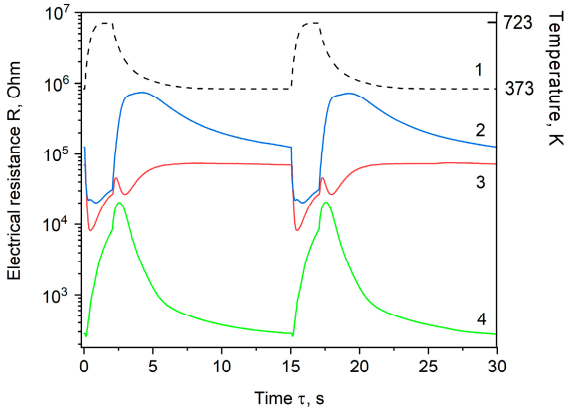

Figure 2. Change in sensor temperature (curve 1) and electrical resistance (curve 2–4) over two measurement cycles for different analyte gases: 2 – carbon monoxide CO, 3 – hydrogen H_2, 4 – hydrogen sulfide H_2S.

3. Results

3.1. Morphological and Composition Characterization

The image of SnO_2 nanopowder obtained by transmission electron microscopy is shown in Figure 3 allow us to estimate the grain size at 7–10 nm.

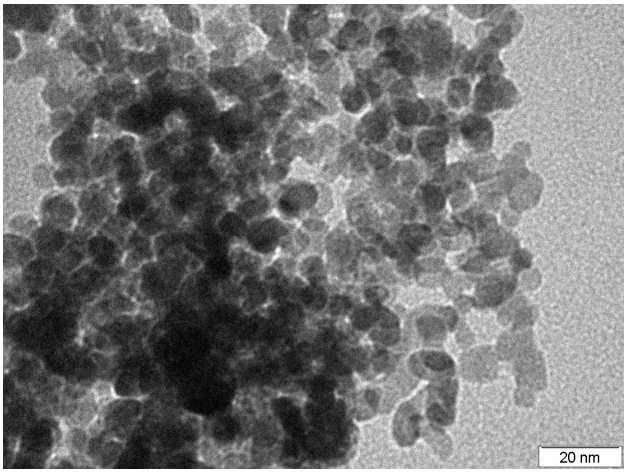

Figure 3. Transmission electron microscopy images of SnO_2 nanopowder.

The diffraction pattern of SnO_2 powder nanoparticles is shown in Figure 4. The left ordinate axis shows the PDF-2 database card information for the tetragonal modification of SnO_2. The experimentally obtained XRD data are shown on the right ordinate axis. It was found that the SnO_2 sample corresponds to the tetragonal SnO_2 phase (PDF card 21–1250). The coherent scattering region estimated using the Debye-Scherrer formula was 5.04 nm.

We have previously shown that the mismatch between the crystallite sizes determined by XRD and the grain size determined by transmission electron microscopy is explained by the composite nature of the grains, which have a core-shell structure [45].

 doi:10.20944/preprints202507.2112.v1

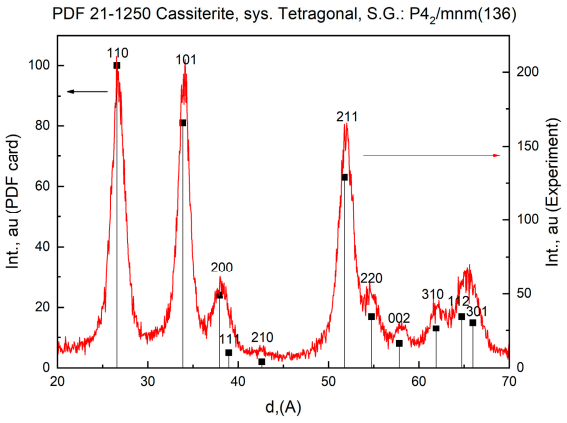

Figure 4. Diffractogram of SnO_2 powder nanoparticles.

3.2. Selective Determination of Hydrogen Sulfide

As shown in Figure 2, each of the analyte gases has its own individual resistance-time dependence, which enables both quantitative and qualitative gas analysis.

Figure 5 shows the change in sensor resistance over one measurement cycle for seven different hydrogen sulfide concentrations in the air. The dots in the figure mark a set of sensor electrical resistance values at a time of 10 seconds from the start of the cycle. Sixty electrical resistance values were taken from each of these seven curves. During the first five seconds of the cycle, when the changes were most significant, electrical resistance values were selected every 0.1 second – a total of 50 values. During the next 10 seconds, electrical resistance values were selected every second – another 10 values were selected. Thus, for each of the curves included in the 15-second measurement cycle, 60 electrical resistance values were selected.

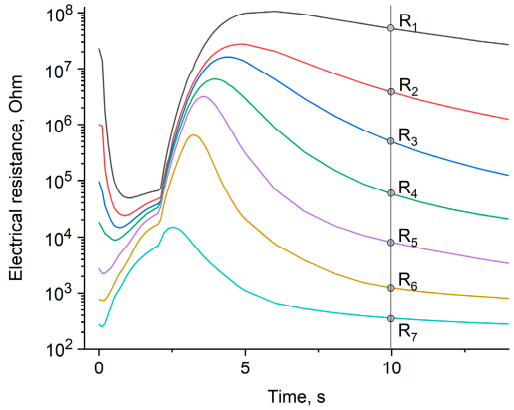

Figure 5. Change in sensor resistance over one measurement cycle for different hydrogen sulfide H_2S concentrations in the air.

The multivariate calibration procedure involves the use of vector quantities, such as, in this case, a set of electrical resistance at different points in time. The calibration dependence obtained from an array of multivariate data is often more accurate than the calibration dependence obtained from a scalar quantity. However, we have slightly modified the standard approach. Usually, regression models are built for electrical resistance from concentration $R = f(\varphi)$. Since our main goal was to synthesize algorithms for an automatic gas analyzer, in order to reduce the number of microcontroller operations, we built regression dependences of concentration on electrical resistance $\varphi = f^{-1}(R)$.

 doi:10.20944/preprints202507.2112.v1

Mathematically, such regression models are equivalent, but by inverting the function, the computational complexity of the algorithm can be reduced.

The empirical coefficients a and b were determined for the power multiplicative model describing the relationship between the observed values of the analyte gas concentration $\{\varphi_i\}$ and the sensor resistance values $\{R_i\}$ at different points in time during the measurement cycle (Figure 6):

$$\varphi_i(R_i|t = 10) = a \cdot R_i^b \cdot \varepsilon_i \text{for } i = 1, 2, \dots, n, \quad (1)$$

where ε_i is the stochastic coefficient corresponding to the deviation of the observed concentration of the analyte gas from its predicted concentration; $n = 60$ is the number of observations in the training part of the sample.

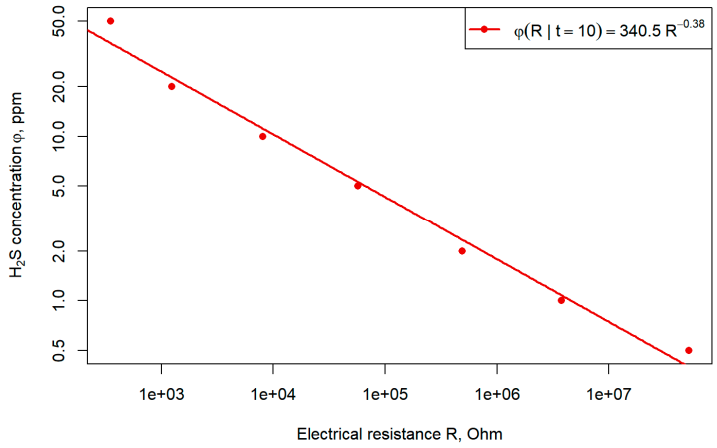

Figure 6. Correlation field for logarithmically scaled concentrations φ of hydrogen sulfide H_2S in air and electrical resistances R of the sensor according to model (1).

Statistical estimates of the coefficients a and b for model (1) were also obtained for other sets $\{\varphi_i(R_i)\}$ of concentrations and electrical resistances of the sensor, corresponding to other moments in the measurement cycle. The training set included a total of 60 sets of sensor resistances with 7 resistance values in each, corresponding to hydrogen sulfide concentrations of 0.5 ppm, 1 ppm, 2 ppm, 5 ppm, 10 ppm, 20 ppm, 50 ppm. Thus, the array of electrical resistance values $\{R_i\}$, containing 420 values, was reduced to an array of coefficients (a, b) of model (1) containing 120 values. Such a reduction allowed not only to compress the training set by factor of 3.5 times, but also to transform it to a form more suitable for subsequent analysis.

To control the quality of the model, a test part of the sample was formed from the data of experiments that were not included in the training part of the sample. In each test, 60 resistance values were used, corresponding to the same points in time as in the training part of the sample. For each of the 60 values of the sensor resistance $\{R_i\}$, the corresponding values of the concentration of the gas-analyte $\{\varphi_i\}$were determined using equation (1) and the previously found coefficients (a, b), while the coefficients and the resistance of the sensor corresponded to the same points in time from the beginning of the measurement cycle. Based on the found concentration values $\{\varphi_i\}$, the sample mean $\bar{\varphi}$ and relative standard deviation S_r were determined. The qualitative analysis procedure was performed by weighing the relative standard deviation with a certain critical value:

$$S_r = \frac{1}{\bar{\varphi}} \sqrt{\frac{1}{m-1} \sum_{j=1}^{m} (\varphi_j - \bar{\varphi})^2} < S_0. \quad (2)$$

In particular, if the relative standard deviation (2) satisfied the inequality H_0: $S_r < 0.45$, then the main hypothesis H_0 was accepted that the analyte is hydrogen sulfideH_2S, otherwise the alternative hypothesis H_1: $S_r \geq 0.45$was accepted that the analyte is any other gas. Analyzing the results of our experiments, we can see that the critical value $S_0 = 0.45$ provides excellent separation of the relative standard deviations for all concentrations of the target gas H_0: $S_r < 0.45$ from the relative standard

 doi:10.20944/preprints202507.2112.v1

deviations for all concentrations of other analyte gases H_0: $S_r \geq 0.45$.As a result, we can formulate an empirical hypothesis that the critical value of the relative standard deviation $S_0 = 0.45$ minimizes the sum of the probabilities of statistical errors of type I and II.

As shown in Figure 7, for all tests with hydrogen sulfide, the relative standard deviation value satisfied the hypothesis H_0: $S_r < 0.45$, and for all tests with other analytes, on the contrary, H_1: $S_r \geq 0.45$. Thus, it was possible to conduct a qualitative analysis for conventionally single-component mixtures of hydrogen sulfide H_2S with air, without statistical errors of types I and II for determination mixtures with air of different concentrations of hydrogen sulfide H_2S (green squares), carbon monoxide CO (blue squares), hydrogen H_2(red squares) or ethanol C_2H_5OH (black squares) entered the research chamber.

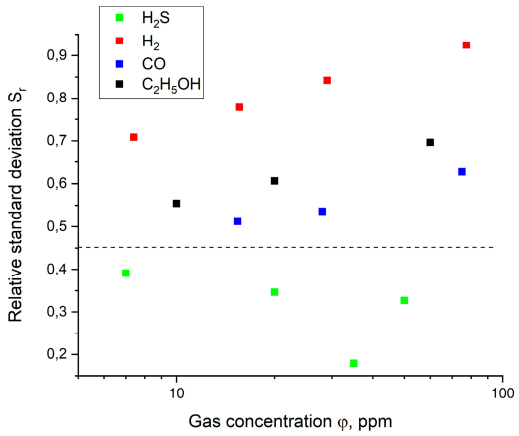

Figure 7. Correlation field for relative standard deviations S_r according to model (1) at different concentrations φ for hydrogen sulfide H_2S and different analyte gases: CO, H_2, C_2H_5OH.

3.3. Selective Determination of Carbon Monoxide

Figure 8 shows the change in sensor resistance during one measurement cycle for seven different concentrations of carbon monoxide in the air. The set of sensor electrical resistance values at 10 seconds from the start of the cycle is marked with dots in the figure. Just as in the selective determination of hydrogen sulfide, sets of empirical coefficients (a, b) were determined for the model (1). By analogy with the training set for hydrogen sulfide H_2S, the training set for carbon monoxide CO included the sensor resistance values $\{R_i\}$ at time t = 10 s corresponding to the following concentrations of CO in the air $\{\varphi_i\}$: 1 ppm, 2 ppm, 5 ppm, 10 ppm, 20 ppm, 50 ppm, 100 ppm.

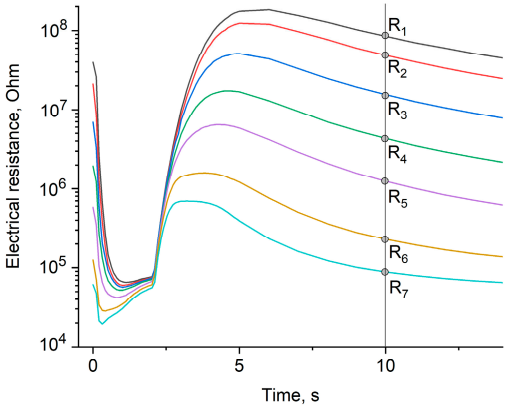

Figure 8. Change in sensor resistance over one measurement cycle for different carbon monoxide CO concentrations in the air.

 doi:10.20944/preprints202507.2112.v1

Experimental data not included in the training set were also used to test the model. As shown in Figure 9, for all tests with carbon monoxide, the relative standard deviation was less than the specified critical level H_0: $S_r < 0.45$, and for all tests with other analytes, the opposite was true H_1: $S_r \geq 0.45$. Thus, it was possible to conduct a qualitative analysis for conventionally single-component mixtures of carbon monoxide with air without statistical errors of types I and II.

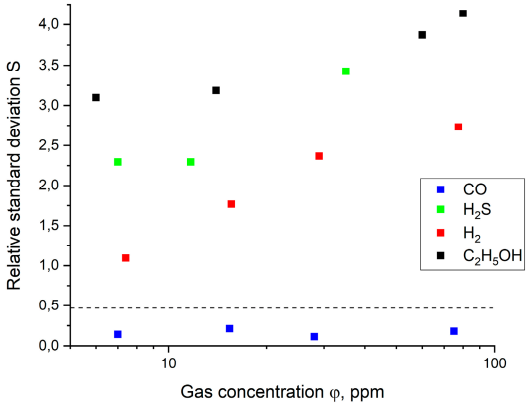

Figure 9. Correlation field for relative standard deviations S_r according to model (1) at different concentrations φ for carbon monoxide CO and different analyte gases: H_2S, H_2, C_2H_5OH.

4. Discussion

The method proposed in this article is a development of the multivariate calibration method, which is widely used for quantitative analysis using multivariate data. In the MCSA method proposed here, when processing test experiment data, in addition to the average concentration value, the relative standard deviation S_r of the concentration values for the analyzed part of the sample is also found. As shown above, the relative standard deviation will not exceed the critical level in $S_r < S_0$ if the test experiment was carried out for the same analyte gas for which the training sample was constructed. However, for other analyte gases, the relative standard deviation will exceed the critical level $S_r \geq S_0$, since the parameters of model (1) were estimated using the training part of the sample for different concentrations of the target components – hydrogen sulfide H_2S and carbon monoxide CO, respectively, which generates a large dispersion in the concentration estimates.

5. Conclusions

Temperature modulation of a semiconductor sensor opens up possibilities for creating a new generation of gas analyzers – inexpensive, compact, providing selective analysis in an autonomous mode in hard-to-reach places. At the same time, existing methods for processing multidimensional sensory data are complex and require sufficiently productive microprocessors for their implementation. The method for processing multidimensional sensory data proposed in this article is quite simple and can be easily implemented using the most economical and energy-efficient mass-produced microcontrollers.

Author Contributions: Conceptualization, A.S., P.M. and A.V.; methodology, A.S. and A.V.; software, A.S. and P.M.; visualization, A.S., P.M. and I.K.; formal analysis, A.S. and P.M.; investigation, A.S., K.O., A.Z., E.V., S.T. and I.K.; writing—original draft preparation, A.S. and P.M.; writing—review and editing, A.S., S.T. and A.V.

Funding: This research was funded by the Ministry of Education and Science of the Russian Federation, project number FSFS-2024-0007.

Acknowledgments: The materials characterization results were obtained on the equipment of the Collective Use Center of Voronezh State University.

 doi:10.20944/preprints202507.2112.v1

Conflicts of Interest: The authors declare no conflicts of interest.

References

1. Shaposhnik, A.V.; Moskalev, P.V.; Chegereva, K.L.; Zviagin, A.A.; Vasiliev, A. Selective Gas Detection of H_2 and CO by a Single MOX-sensor. *Sens. Actuators B: Chem.* **2021**, *334*, 129376, https://doi.org/10.1016/J.SNB.2020.129376.
2. Heilig, A.; Bârsan, N.; Weimar, U.; Schweizer-Berberich, M.; Gardner, J.W.; Göpel, W. Gas Identification by Modulating Temperatures of SnO_2-Based Thick Film Sensors. *Sens. Actuators B: Chem.* **1997**, *43*, 45, https://doi.org/10.1016/S0925-4005(97)00096-8.
3. Nakata, S.; Okunishi, H.; Nakashima, Y. Distinction of Gases with a Semiconductor Sensor Depending on the Scanning Profile of a Cyclic Temperature. *Analyst* **2006**, *131*, 148, https://doi.org/10.1039/B509996J.
4. Krivetskiy, V.; Efitorov, A.; Arkhipenko, A.; Vladimirova, S.A.; Rumyantseva, M.; Dolenko, S.; Gaskov, A. Selective Detection of Individual Gases and CO/H_2 Mixture at Low Concentrations in Air by Single Semiconductor Metal Oxide Sensors Working in Dynamic Temperature Mode. *Sens. Actuators B: Chem.* **2018**, *254*, 502, https://doi.org/10.1016/J.SNB.2017.07.100.
5. Shaposhnik, A.V.; Moskalev, P.V.; Arefieva, O.A.; Zviagin, A.A.; Kul, O.V.; Vasiliev, A.V. Selective Determination of Hydrogen in a Mixture with Methane Using a Single Metal Oxide Sensor. *Int. J. Hydrog. Energy* **2024**, *82*, 523, https://doi.org/10.1016/j.ijhydene.2024.07.379.
6. Shaposhnik, A.V.; Moskalev, P.V.; Zviagin, A.A.; Duykova, M.V.; Ryabtsev, S.V.; Ghareeb, D.A.A.; Vasiliev, A.A. Selective Determination of Hydrogen Sulfide Using SnO_2–Ag Sensor Working in Non-Stationary Temperature Regime. *Chemosensors* **2021**, *9*, 203. https://doi.org/10.3390/chemosensors9080203.
7. Noh, H.W.; Jang, Y.; Park, H.D.; Kim, D.; Choi, J.H.; Ahn, C.-G. A Selective Feature Optimized Multi-Sensor Based e-Nose System Detecting Illegal Drugs Validated in Diverse Laboratory Conditions. *Sens. Actuators B: Chem.* **2023**, *390*, 133965, https://doi.org/10.1016/j.snb.2023.133965.
8. Haddi, Z.; Amari, A.; Ali, A.Ould.; Bari, N.E.; Barhoumi, H.; Maaref, A.; Jaffrezic-Renault, N.; Bouchikhi, B. Discrimination and Identification of Geographical Origin Virgin Olive Oil by an E-Nose Based on MOS Sensors and Pattern Recognition Techniques. *Procedia Eng.* **2011**, *25*, 1137, https://doi.org/10.1016/j.proeng.2011.12.280.
9. Anyfantis, A.; Silis, A.; Blionas, S. A Low Cost, Mobile e-Nose System with an Effective User Interface for Real Time Victim Localization and Hazard Detection in USaR Operations. *Meas. Sens.* **2021**, *16*, 100049, https://doi.org/10.1016/j.measen.2021.100049.
10. Fedorov, F.S.; Simonenko, N.P.; Trouillet, V.; Volkov, I.A.; Plugin, I.A.; Rupasov, D.P.; Mokrushin, A.S.; Nagornov, I.A.; Simonenko, T.L.; Vlasov, I.S.; et al. Microplotter-Printed On-Chip Combinatorial Library of Ink-Derived Multiple Metal Oxides as an "Electronic Olfaction" Unit. *ACS Appl. Mater. Interfaces* **2020**, *12*, 56135, https://doi.org/10.1021/acsami.0c14055.
11. Bobkov, A.; Varezhnikov, A.; Plugin, I.; Fedorov, F.S.; Trouillet, V.; Geckle, U.; Sommer, M.; Goffman, V.; Moshnikov, V.; Sysoev, V. The Multisensor Array Based on Grown-On-Chip Zinc Oxide NanoRoD Network for Selective Discrimination of Alcohol Vapors at Sub-Ppm Range. *Sensors* **2019**, *19*, 4265, https://doi.org/10.3390/s19194265.
12. Rescalli, A.; Marzorati, D.; Gelosa, S.; Cellesi, F.; Cerveri, P. Temperature Modulation of MOS Sensors for Enhanced Detection of Volatile Organic Compounds. *Chemosensors* **2023**, *11*, 501, https://doi.org/10.3390/chemosensors11090501.
13. Iwata, T.; Saeki, M.; Okura, Y.; Yoshikawa, T. Gas Discrimination Based on Enhanced Gas-Species Related Information Obtained by a Single Gas Sensor with Novel Temperature Modulation. *Sens. Actuators B: Chem.* **2021**, *354*, 131225, https://doi.org/10.1016/j.snb.2021.131225.
14. Burgués, J.; Marco, S. Multivariate Estimation of the Limit of Detection by Orthogonal Partial Least Squares in Temperature-Modulated MOX Sensors. *Anal. Chim. Acta* **2018**, *1019*, 49, https://doi.org/10.1016/j.aca.2018.03.005.
15. Herrero-Carrón, F.; Yáñez, D.J.; De Borja Rodríguez, F.; Varona, P. An Active, Inverse Temperature Modulation Strategy for Single Sensor Odorant Classification. *Sens. Actuators B: Chem.* **2014**, *206*, 555, https://doi.org/10.1016/j.snb.2014.09.085.

 doi:10.20944/preprints202507.2112.v1

16. Nakata, S.; Takahara, N. Distinction of Gaseous Mixtures Based on Different Cyclic Temperature Modulations. *Sens. Actuators B: Chem.* **2022**, *359*, 131615, https://doi.org/10.1016/j.snb.2022.131615.
17. Fan, H.; Jia, X. Selective Detection of Acetone and Gasoline by Temperature Modulation in Zinc Oxide Nanosheets Sensors. *Solid State Ion.* **2010**, *192*, 688, https://doi.org/10.1016/j.ssi.2010.05.058.
18. Meng, F.; He, L.; Ji, H.; Yuan, Z. Sawtooth Wave Temperature Modulation Measurement Method for Recognizing Five Kinds of VOCs Based on ZnO Gas Sensor. *Meas.* **2024**, *228*, 114342, https://doi.org/10.1016/j.measurement.2024.114342.
19. Gosangi, R.; Gutierrez-Osuna, R. Active Temperature Modulation of Metal-Oxide Sensors for Quantitative Analysis of Gas Mixtures. *Sens. Actuators B: Chem.* **2013**, *185*, 201, https://doi.org/10.1016/j.snb.2013.04.056.
20. Fernandez, L.; Guney, S.; Gutierrez-Galvez, A.; Marco, S. Calibration Transfer in Temperature Modulated Gas Sensor Arrays. *Sens. Actuators B: Chem.* **2016**, *231*, 276, https://doi.org/10.1016/j.snb.2016.02.131.
21. Ionescu, R.; Llobet, E.; Brezmes, J.; Vilanova, X.; Correig, X. Dealing with Humidity in the Qualitative Analysis of CO and NO_2 Using a WO_3 Sensor and Dynamic Signal Processing. *Sens. Actuators B: Chem.* **2003**, *95*, 177, https://doi.org/10.1016/s0925-4005(03)00411-8.
22. Vergara, A.; Llobet, E.; Brezmes, J.; Ivanov, P.; Cané, C.; Gràcia, I.; Vilanova, X.; Correig, X. Quantitative Gas Mixture Analysis Using Temperature-Modulated Micro-Hotplate Gas Sensors: Selection and Validation of the Optimal Modulating Frequencies. *Sens. Actuators B: Chem.* **2006**, *123*, 1002, https://doi.org/10.1016/j.snb.2006.11.010.
23. Ding, H.; Ge, H.; Liu, J. High Performance of Gas Identification by Wavelet Transform-Based Fast Feature Extraction from Temperature Modulated Semiconductor Gas Sensors. *Sens. Actuators B: Chem.* **2005**, *107*, 749, https://doi.org/10.1016/j.snb.2004.12.009.
24. Di Giuseppe, D.; Catini, A.; Comini, E.; Zappa, D.; Di Natale, C.; Martinelli, E. Optimizing MOX Sensor Array Performances with a Reconfigurable Self-Adaptive Temperature Modulation Interface. *Sens. Actuators B: Chem.* **2021**, *333*, 129509, https://doi.org/10.1016/j.snb.2021.129509.
25. Deng, Q.; Gao, S.; Lei, T.; Ling, Y.; Zhang, S.; Xie, C. Temperature & Light Modulation to Enhance the Selectivity of Pt-Modified Zinc Oxide Gas Sensor. *Sens. Actuators B: Chem.* **2017**, *247*, 903, https://doi.org/10.1016/j.snb.2017.03.107.
26. Huang, X.-J.; Choi, Y.-K.; Yun, K.-S.; Yoon, E. Oscillating Behaviour of Hazardous Gas on Tin Oxide Gas Sensor: Fourier and Wavelet Transform Analysis. *Sens. Actuators B: Chem.* **2005**, *115*, 357, https://doi.org/10.1016/j.snb.2005.09.022.
27. Nakata, S.; Neya, K.; Takemura, K.K. Non-Linear Dynamic Responses of a Semiconductor Gas Sensor — Competition Effect on the Sensor Responses to Gaseous Mixtures. *Thin Solid Films* **2001**, *391*, 293, https://doi.org/10.1016/s0040-6090(01)00998-1.
28. Kato, Y.; Mukai, T. A Real-Time Intelligent Gas Sensor System Using a Nonlinear Dynamic Response. *Sens. Actuators B: Chem.* **2006**, *120*, 514, https://doi.org/10.1016/j.snb.2006.03.021.
29. Ge, H.; Liu, J. Identification of Gas Mixtures by a Distributed Support Vector Machine Network and Wavelet Decomposition from Temperature Modulated Semiconductor Gas Sensor. *Sens. Actuators B: Chem.* **2005**, *117*, 408, https://doi.org/10.1016/j.snb.2005.11.037.
30. Olivieri, A.C. Handling Non-Linearities and Pre-Processing in Multivariate Calibration of Vibrational Spectra. *Microchem. J.* **2024**, 112323, https://doi.org/10.1016/j.microc.2024.112323.
31. Iurgenson, N.; Monakhova, Y.; Kirsanov, D. Multivariate Calibration Transfer between ATR-FTIR and NIR Spectrometers: Electronic Cigarette Refill Fluids Case Study. *Microchem. J.* **2025**, 113375, https://doi.org/10.1016/j.microc.2025.113375.
32. Ahumada, F.D.A.; Acevedo, I.; Magkanas, G.; Palomar, T.; Pastor, P.; Saurina, J.; García, J.F. Multivariate Calibration Strategies for Improved Elemental Determination of Heritage Glass Objects by Using Portable X-Ray Fluorescence. *Microchem. J.* **2025**, 113838, https://doi.org/10.1016/j.microc.2025.113838.
33. Yeganeh, F.N.; Bahram, M.; Olivieri, A.C.; Abdollahi, H. Area of Feasible Figures of Merit (AF-FOMs) for Second-Order Multivariate Calibrations in Multivariate Curve Resolution (MCR). *Anal. Chim. Acta* **2024**, *1319*, 342987, https://doi.org/10.1016/j.aca.2024.342987.

 doi:10.20944/preprints202507.2112.v1

34. Tanzilli, D.; Strani, L.; Metz, M.; Roger, J.M.; Lesnoff, M.; Ruckebusch, C.; Cocchi, M.; Vitale, R. Locally-Weighted-RoBoost-PLS: A Multivariate Calibration Approach to Simultaneously Cope with Non-Linearities and Outliers. *Anal. Chim. Acta* **2025**, *1362*, 344167, https://doi.org/10.1016/j.aca.2025.344167.
35. Rexhepi, F.; Surleva, A.; Gjinovci, V. Application of FTIR Spectroscopy and Multivariate Calibration for Prediction of Acrylamide in Potato Chips Commercial Samples. *Spectrochim. Acta A Mol. Biomol. Spectrosc.* **2024**, 125655, https://doi.org/10.1016/j.saa.2024.125655.
36. Cai, L.; Zhu, S.; Wu, G.; Jiao, F.; Li, W.; Wang, X.; An, Y.; Hu, Y.; Sun, J.; Dong, X.; et al. Highly Sensitive H_2 Sensor Based on PdO-Decorated WO_3 Nanospindle p-n Heterostructure. *Int. J. Hydrogen Energy* **2020**, *45*, 31327, https://doi.org/10.1016/j.ijhydene.2020.08.109.
37. Mineo, G.; Moulaee, K.; Neri, G.; Mirabella, S.; Bruno, E. H_2 Detection Mechanism in Chemoresistive Sensor Based on Low-Cost Synthesized WO_3 Nanorods. *Sens. Actuators B: Chem.* **2021**, *348*, 130704, https://doi.org/10.1016/j.snb.2021.130704.
38. Zhou, R.; Lin, X.; Xue, D.; Zong, F.; Zhang, J.; Duan, X.; Li, Q.; Wang, T. Enhanced H_2 Gas Sensing Properties by Pd-Loaded Urchin-like $W_{18}O_{49}$ Hierarchical Nanostructures. *Sens. Actuators B: Chem.* **2018**, *260*, 900, https://doi.org/10.1016/j.snb.2018.01.104.
39. Kim, H.; Pak, Y.; Jeong, Y.; Kim, W.; Kim, J.; Jung, G.Y. Amorphous Pd-Assisted H_2 Detection of ZnO Nanorod Gas Sensor with Enhanced Sensitivity and Stability. *Sens. Actuators B: Chem.* **2018**, *262*, 460, https://doi.org/10.1016/j.snb.2018.02.025.
40. Meng, X.; Bi, M.; Xiao, Q.; Gao, W. Ultra-Fast Response and Highly Selectivity Hydrogen Gas Sensor Based on Pd/SnO_2 Nanoparticles. *Int. J. Hydrogen Energy* **2021**, *47*, 3157, https://doi.org/10.1016/j.ijhydene.2021.10.201.
41. Liewhiran, C.; Tamaekong, N.; Wisitsoraat, A.; Tuantranont, A.; Phanichphant, S. Ultra-Sensitive H_2 Sensors Based on Flame-Spray-Made Pd-Loaded SnO_2 Sensing Films. *Sens. Actuators B: Chem.* **2012**, 176, 893, https://doi.org/10.1016/j.snb.2012.10.087.
42. Qiu, T.; Zhou, S.; Ji, J.; Wu, G.; Yan, W.; Ling, M.; Liang, C. High Performance H_2 Sensor Based on rGO-Wrapped SnO_2–Pd Porous Hollow Spheres. *Ceram. Int.* **2022**, *48*, 15056, https://doi.org/10.1016/j.ceramint.2022.02.034.
43. Zhang, S.; Yin, C.; Yang, L.; Zhang, Z.; Han, Z. Investigation of the H_2 Sensing Properties of Multilayer Mesoporous Pure and Pd-Doped SnO_2 Thin Film. *Sens. Actuators B: Chem.* **2018**, *283*, 399, https://doi.org/10.1016/j.snb.2018.12.051.
44. Meng, X.; Bi, M.; Gao, W. Rapid Response Hydrogen Sensor Based on Pd@Pt/SnO_2 Hybrids at near-Ambient Temperature. *Sens. Actuators B: Chem.* **2022**, *370*, 132406, https://doi.org/10.1016/j.snb.2022.132406.
45. Shaposhnik, A.V.; Shaposhnik, D.A.; Turishchev, S.Y.; Chuvenkova, O.A.; Ryabtsev, S.V.; Vasiliev, A.A.; Vilanova, X.; Hernandez-Ramirez, F.; Morante, J.R. Gas Sensing Properties of Individual SnO_2 Nanowires and SnO_2 Sol–Gel Nanocomposites. *Beilstein J. Nanotechnol.* **2019**, *10*, 1380, https://doi.org/10.3762/bjnano.10.136.